Electrical spin injection in metallic mesoscopic spin valves

Jedema, Friso

Chapter 3

Experimental techniques and sample fabrication

3.1 Introduction

The discovery of several new phenomena in mesoscopic physics is a direct result from the advances obtained in the fabrication of nanometer scale devices in the last two decades. One of the most important factors has been the development of electron beam lithography, EBL, which uses a focussed beam of high energy electrons to expose an electron sensitive resist on a suitable substrate. The short wavelength of the high energy electrons enables fabrication of devices with a much higher resolution ($\sim$ 50 nm) than those fabricated using optical lithography techniques. This accuracy makes EBL a well suited technique to pattern structures which are smaller than the relevant length scale for studying spin dependent electron transport in metals. In nonmagnetic metals the relevant length scale for spin injection is the spin relaxation length, which for thin metallic films is of the order of 1 μm.

3.2 Sample fabrication techniques

In this paragraph the techniques necessary to fabricate the devices presented in the remainder of this work are discussed. After a short introduction on the principle of electron beam lithography in §3.2.1, a description of the fabrication of two different resist systems which can be used in the metal deposition processes discussed is given in §3.2.2. In the last paragraph the method to remove the resist after evaporation (lift-off) is discussed.

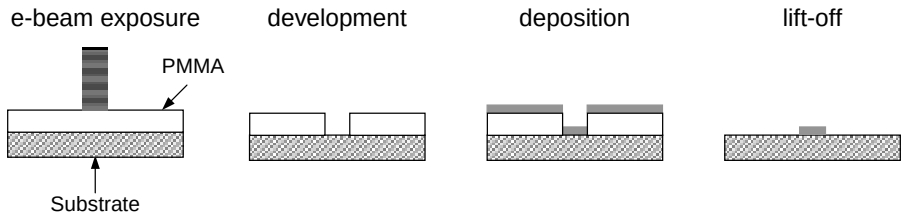

Figure 3.1: *Schematic description of the lift-off process. An electron sensitive resist is exposed to a high energy electron beam (left). The exposed areas are dissolved in a suitable developer and material is deposited on top of the remaining resist structure (two center images). As a last step the sample is put in a strong solvent that removes all resist. Material deposited on top of the resist is hence removed (right).*

3.2.1 Electron beam lithography, EBL

The first EBL machines were developed in the late 1960s. Shortly thereafter came the discovery that a common polymer, polymethyl methacrylate (PMMA), made an excellent e-beam resist [1]. Despite sweeping technological advances, PMMA is still the most commonly used e-beam resist. The main advantages of EBL are high resolution and great flexibility. Designs for devices can be made in a computer program and directly used to expose a sample. The time consuming step of mask making necessary for optical lithography is not needed. These advantages make it the most commonly used patterning method in a research environment. The most important drawback, low speed, which is crucial in an industrial environment, is less applicable here. All essential elements of the samples discussed in this work have been fabricated using EBL with a 37 keV electron beam generated by a customized JEOL 840 scanning electron microscope (SEM) and equipped with software from Raith Gmbh. With this system resolution to a line width of 50 nm is possible. The general principle of the sample fabrication is shown in Fig. 3.1. An electron sensitive resist mostly based on PMMA is applied on top of a (silicon) substrate by spin coating and drying on a hot plate. Subsequently a predefined pattern is exposed using the high energy electron beam with the result that polymer chains exposed to the electron beam are broken and become soluble in a suitable developer [2]. The maximum resolution obtained in the system is not determined by the diameter of the electron beam nor the by the electron wave length but by scattering and subsequent broadening of the electron beam in the resist (forward scattering) and scattering of the electron beam in the substrate and subsequent reflection back into the resist (backscattering). The latter gives rise to secondary exposure of the resist, which is especially strong near large exposed areas. This proximity effect makes EBL a non-straightforward technique

for complex patterning [3]. After the e-beam exposure, the sample is put in a suitable developer which removes the exposed areas of the resist. The next step is the material deposition. E-gun evaporation is used to deposit the various metals, except for permalloy $Ni_{80}Fe_{20}$ (Py), which is deposited using DC sputtering in a argon environment. The Py layers are sputtered at IMEC (Belgium). After deposition, the sample is put in a solvent, usually heated acetone, to remove the polymer and the metal on top of it. This technique is called lift-off.

3.2.2 Creating an evaporation mask using electron beam lithography

In this thesis two different resist systems in combination with e-beam lithography to fabricate our samples are used: a conventional PMMA bi-layer system for conventional metal deposition using evaporation or sputtering and a tri-layer system using a PMMA-MA ballast layer, a germanium (Ge) middle layer and PMMA top layer used for shadow evaporation techniques. In Fig. 3.2 the fabrication procedure of the two resist systems is described. The used substrate for all experiments is a single side polished P-doped Si $< 100 >$ wafer ($\rho = 100 - 200\ \Omega cm$) with a thermally grown oxide of approximately 200 nm.

Conventional PMMA bi-layer

This technique represents the standard and most widely used resist system for electron beam lithography. The substrate is covered with two layers of PMMA using spin coating and baking on a hot plate. The layers have a different molecular weight with the heaviest compound on top. This has the advantage of forming a better, i.e. slightly overhanging, resist profile, as shown in the top right part of Fig. 3.2. Such a profile is important for a good lift off, especially in the case of DC sputtering. The following process is used to create the PMMA bi-layer:

Bottom layer: Du Pont Elvacite PMMA 2010 (medium molecular weight), 4% in chlorobenzene, filtered with 0.2 μm filters and spun at 4000 rpm for 70 seconds depending on the desired resist height. Subsequently, the resist is baked for 10 minutes on a hot plate at 170°C.

Top layer: Du Pont Elvacite PMMA 2041 (very high molecular weight), 2% in O-xylene using the same spin speed and baking settings. For the highest possible resolution, hardness and best resist profile, a time of 3 hours is used for baking on a hot plate at 170°C. It is important to use for this top layer a rather weak solvent, such as O-xylene, to prevent intermixing of the

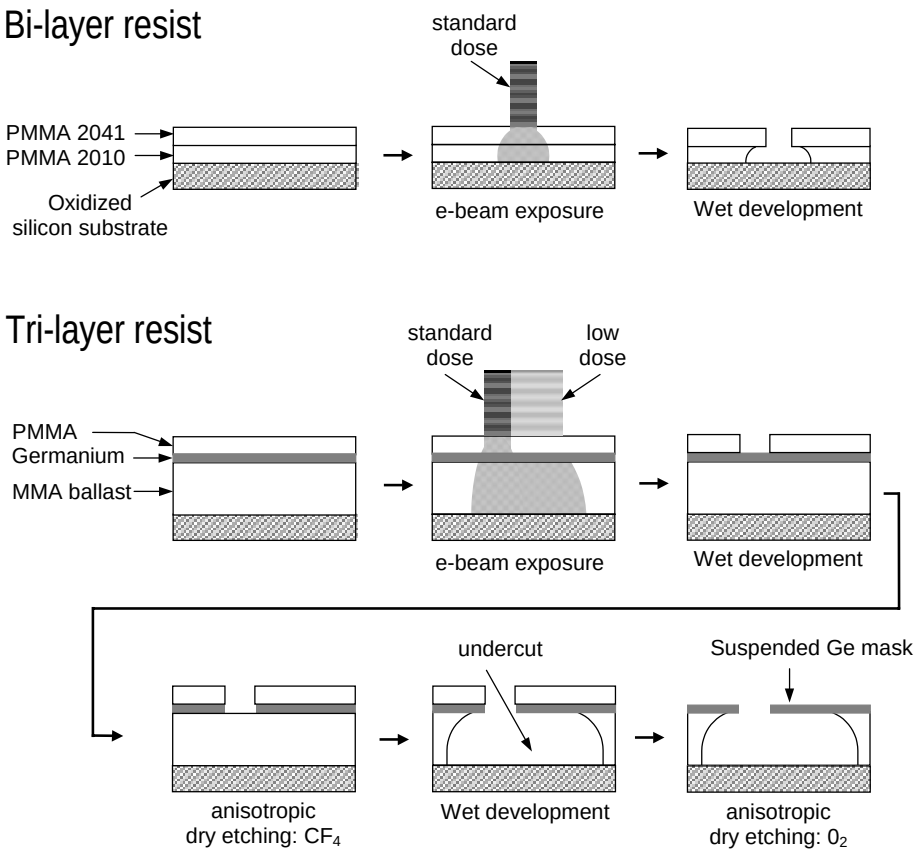

Figure 3.2: *Schematic representation of the two different lithographic systems used in this thesis for the fabrication of the spin injection devices. The top row shows the process of making a conventional PMMA bi-layer system. The middle and bottom rows show the more complex fabrication of tri-layer system and the creation of a suspended germanium (Ge) layer with well defined undercuts used for shadow evaporation techniques.*

two layers during application of the second layer. The typical thickness for each layer is about 150 nm, making the total thickness of the bi-layer about 300 nm [4].

The sample is exposed using a 37 keV electron beam with a typical dose of 200 μCcm^{-2}. Smaller structures with a line width of $\sim$ 100 nm typically need twice this dose. Subsequently a wet development step is carried out for 50 seconds in a 3:1 mixture of IPA:MIBK (2-propanol:methyl-isobutyl-ketone) and flushed for 60 seconds in IPA. As a last step a short anisotropic oxygen etch is done in a reactive ion etcher to remove the last PMMA remnants left on the substrate: Oxygen pressure 9 μBar, Power = 40 W, etch time: 20 seconds.

PMMA-germanium-MA trilayer

This recipe is used for the fabrication of spin injection devices with a shadow evaporation technique [5]. Shadow evaporation is a necessary technique to be able to fabricate tunnel barrier contacts in a controlled way and will be discussed in §3.2.3. The process of fabricating the tri-layer resist system is schematically shown in the middle and bottom rows of Fig. 3.2.

Bottom layer: Allresist GMBH ARP 680.10 PMMA-MA (in methoxy-ethanol). The spin speed determines the thickness of the resist: 2000 rpm gives a thickness of 1.2 μm. The spin time is 70 seconds and baking is 20 minutes at 170°C on a hot plate.

Germanium layer: The germanium (Ge) layer is put on top of the bottom PMMA-MA layer by e-gun evaporation at a rate of 0.1-0.2 nm/s in a high vacuum system with a background pressure of $1 \cdot 10^{-7}$mbar. The thickness of the Ge layer is 40 nm.

Top layer: Allresist GMBH ARP 671.04 PMMA (in chlorobenzene). Spin speed is determined again by the desired layer thickness: 4000 rpm gives a thickness of 400 nm. The spin time is 70 seconds and baking is 20 minutes at 150°C on a hot plate.

The deposition of the PMMA-MA bottom layer and the PMMA top layer is identical to the procedure described in the previous paragraph, except for the fact that the top layer is now baked at 150°C in stead of 170°C. The baking temperature of the top layer is lower than that of the bottom layer because otherwise out-gassing from the bottom layer will cause a cracking of the Ge layer.

To expose both resist layers a typical (high) dose of 200 μCcm^{-2} necessary, whereas for the exposure of only the PMMA-MA bottom layer a typical (low) dose of 100 μCcm^{-2} is used. After e-beam exposure the sample is developed for 40 seconds in 3:1 IPA:MIBK with a 60 second stop in IPA. The top layer is developed only where it has received the high dose. The pattern in the top layer is now transferred into the Ge by means of an anisotropic dry etch in a reactive ion etcher using the following settings: CF_4 gas with a pressure $P = 25\ \mu Bar$ at 40 W for about 40 seconds. The exact etch time is monitored using a laser interferometer to prevent over-etching, which causes a decrease in resolution of the line width. Subsequently the bottom layer is developed for 40 seconds in 5:1 IPA:MIBK with a 10 second stop in IPA and a 30 second stop in demi-water. Both bottom resist regions, having received either a normal dose or a low dose, are developed in this step. As a last

step the remaining resist on top of the germanium is completely removed using an oxygen plasma at 9 μBar with 40 W power for 3 minutes. Due the complete removal of the top resist layer a minimum thickness of the suspended mask is obtained, being limited by the thickness of the Ge layer.

3.2.3 Metal deposition

After completion of the mask, three different methods have been used to deposit metals: electron gun evaporation, electron gun evaporation in combination with shadow evaporation and DC sputtering.

Electron gun evaporation

Electron gun evaporation is a thermal evaporation process. The sample is placed on a sample holder which is positioned upside down in a vacuum chamber. On the bottom of the chamber a rotatable source is present containing 4 different source metals: nickel (Ni), cobalt (Co), germanium (Ge) and aluminum (Al). A high energy electron beam is used to heat one of the metals, which evaporates and condenses on the sample facing the heated metal source. In between the sample and the metal source a shutter is positioned functioning as a on/off switch to control the deposition. The deposition rates are typical in the order of 0.1 - 1 nm/s for the above mentioned metals. The higher the evaporation speed and the lower the pressure, the cleaner the film. The main advantages of e-gun evaporation are high power, so that materials with high melting points can be evaporated. Another advantage is the fact that evaporation in vacuum is highly anisotropic, i.e. in one specific direction. This property enables the deposition process called shadow evaporation. The base pressure of the system is $2 \cdot 10^{-7}$ mbar.

Shadow evaporation

For shadow evaporation a sample holder is used that can be tilted and rotated in combination with a resist system with undercuts as can be seen in Fig. 3.2, see also Refs. [5, 6]. Due to the anisotropic nature of the deposition by e-gun evaporation, different projections of an opening in the mask can be deposited without breaking the vacuum. The principle is shown in the left panel of Fig. 3.3 where two depositions are done with two different angles to the substrate: one perpendicular and one at an angle θ. As a result two projections are deposited on the substrate a distance d apart. If a second projection is not desired at a specific location the undercut can be made smaller at that point, as shown in the right panel of Fig. 3.3. At sufficient large angles θ' the material is then deposited in the side wall of the resist, resulting in a removal upon lift-off. An advantage of shadow evaporation is that it allows one to fabricate complex structures consisting

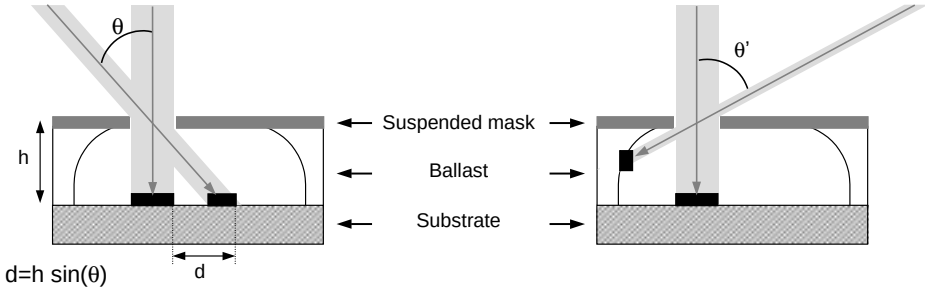

Figure 3.3: *The principle of shadow evaporation. By evaporating in two steps with a difference in angle θ through a resist system with a suspended mask, structures can be shifted with respect to each other by a distance d (left picture). Also structures can be prevented to be deposited on the substrate by using large angles θ' and smaller undercuts. This results into a projection into the side wall of the resist and therefore removal upon lift-off (right picture).*

of two different metals without taking the sample out of the evaporation chamber. In particular, by using aluminum as one of the metals the shadow evaporation technique facilitates a control of the interface transparency of the contacts from fully transparent ($T \approx 0.5$) to the tunnel barrier regime ($T \approx< 5 \cdot 10^{-5}$) by exposing the aluminum to oxygen after deposition.

Sputtering

For metallic alloys, where a well defined stoichiometry is desired, another method for deposition is used. For the deposition of permalloy $Ni_{80}Fe_{20}$ (Py) DC magnetron sputtering with a low pressure argon plasma is used in combination with the conventional PMMA bi-layer resist. The sputtering of the Py layers has been done at IMEC (Belgium) in the group of G. Borghs and J. de Boeck. A drawback of sputtering is the fact that it is isotropic, which demands a better (more overhanging) resist profile than evaporation. If this condition is not met, very high 'ears' are formed at structure edges, which can cause major problems if a good step coverage of the sputtered Py layer is needed by in a second deposition step.

3.2.4 Lift-off

The last step in the process is lift off. For delicate samples in which metals are used with relatively poor adhesion, such as copper, the sample is immersed in boiling acetone until all residual material has lifted off. Then it is flushed in cold ethanol and the sample is spin dried. For more robust samples, such as Al, Co, Ni and sputter deposited Py with a tantalum (Ta) adhesion layer, ultrasonic agitation in heated acetone can be used. Ultra-

sonic agitation in combination with the stronger (heated) solvent J.T.Baker PRS 3000 resist stripper can be important, especially after sputter deposition of the Py metal, to remove resist 'ears' at the edges of a structure.

3.3 Interface quality

3.3.1 Transparent interfaces

As discussed previously, shadow evaporation can be used to deposit different layers without breaking the vacuum. This guarantees a transparent interface if the back ground pressure is sufficiently low. A metallic interface is considered highly transparent when the interface resistance is indistinguishable from the metallic bulk diffusive resistance over an elastic mean free path.

However, shadow evaporation is not always possible, for example in the case of Py sputter deposition. In this case a two or more step process is used, in which every metal layer is deposited using a different lithography step. Hence the surface of the first layer is exposed to the ambient atmosphere for a prolonged period causing contamination and the possible formation of oxides. To create a highly transparent interface between two metal layers, two cleaning steps are necessary prior to the deposition of the second layer. First an oxygen plasma etch is applied to remove PMMA remnants from the surface. This is included in every resist fabrication step. Secondly an *in situ* etch with an inert gas is applied prior to the deposition of the second metal.

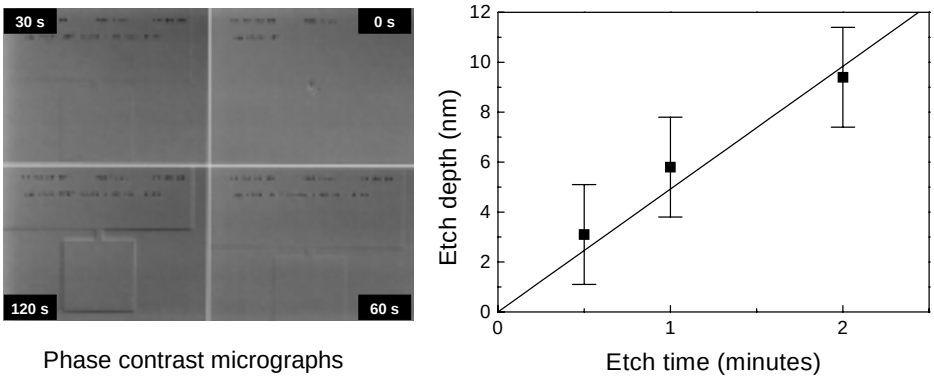

Figure 3.4: *Etch depth as a function of etch time for a 40 nm thick Py film. The linear fit through the origin yields an etching rate of 5 nm/minute. The micrographs on the left show the etched steps as observed by optical phase contract microscopy at 100 X magnification*

The native oxide present at the surface of the Py, Co or Ni metals can be removed by ion beam milling or Kaufmann etching. A typical etch of

about 30 seconds at an argon (Ar) pressure of $2 \cdot 10^{-4}$ mbar, an acceleration beam voltage of 500 eV and an etch current of 1.3 ± 0.1 mA is sufficient to remove a few nm of metal. This was verified by measuring the height profile of lithographically patterned steps in 40 nm thick Py and Co films with a Dektak^{3}ST surface profile measuring system. Interestingly, the etched steps of only a few nm height could also be observed with a phase contrast microscope. In Fig. 3.4 a plot is shown of the etch depth versus etch time for Py, as well as photographs of the etched pattern as observed by phase contrast microscopy at 100 X magnification.

3.3.2 Tunnel barrier junctions

In some cases a tunnel barrier between two metallic layers is desired. There are many ways to fabricate tunnel barriers, however the use of aluminium oxide (Al_2O_3) as a tunnel barrier material is particularly easy from a fabrication point of view and it has proven itself as a reliable barrier over many years in superconducting tunneling experiments [7] and in ferromagnetic tunnel junctions [8]. In this work an $Al/Al_2O_3/Co$ nonmagnetic metal-tunnel barrier-ferromagnetic metal system is used for spin injection and detection. The fabrication procedure is based upon shadow evaporation. In the first step aluminium is deposited by e-gun evaporation through a suspended mask. Next, without breaking the vacuum, pure O_2 is let into the vacuum system for 10 minutes and an Al_2O_3 oxide layer is formed. Guided by a rather extensive investigation of the contact resistance for $Al/Al_2O_3/Cu$ junctions by Baselmans [9], the $Al/Al_2O_3/Co$ tunnel junctions are exposed to three different pressures ($5 \cdot 10^{-3}$ $mbar$, $1 \cdot 10^{-2}$ $mbar$) and $5 \cdot 10^{-2}$ $mbar$ for 10 minutes each, to determine the tunnel barrier quality and the contact resistance as a function of oxygen exposure (O_2 pressure times oxidation time). In Fig. 3.5 the resulting contact resistance is shown as a function of oxygen exposure together with the results for $Al/Al_2O_3/Cu$ junctions as obtained by Baselmans [9].

For all oxygen exposures of 3, 6 and 30 $mbar \cdot s$ an increase of the $Al/Al_2O_3/Co$ junction contact resistance of about 10 % is observed upon cooling from RT to liquid He temperature. This is, in combination with the quadratic dependence of the resistance on the DC voltage bias as shown in the top right graph of Fig. 3.5, a good indication that the dominant transport process from the Al to the Co is electron tunnelling [10, 12, 13]. The same behavior was observed for the $Al/Al_2O_3/Cu$ junctions except for the data point at 6 $mbar \cdot s$, for which the observed quadratic dependence of the resistance upon voltage bias changes sign and becomes much weaker. Also the increase in resistance upon cooling to liquid He temperature for this sample disappears, indicating that the $Al/Al_2O_3/Cu$ tunnel barrier is probably suffering from pinhole leakage currents. The shift in voltage

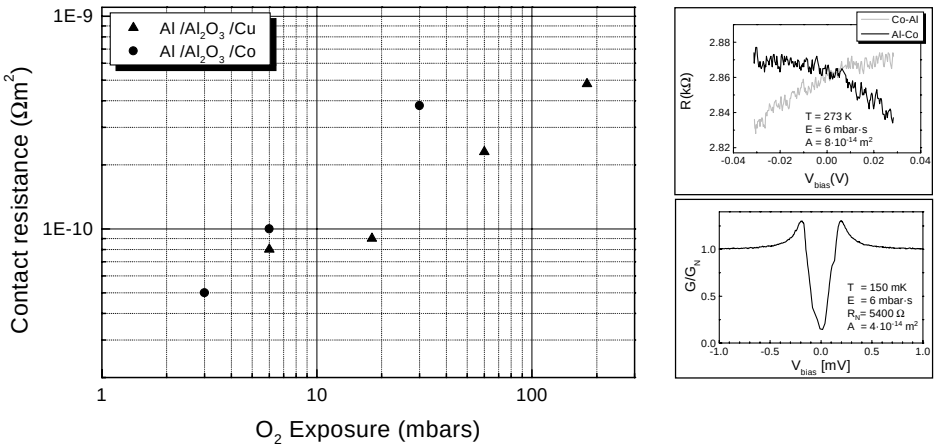

Figure 3.5: *Contact resistance at 4.2 K of $Al/Al_2O_3/Cu$ and $Al/Al_2O_3/Co$ tunnel junctions as a function of oxygen exposure (pressure multiplied by time). In all cases the oxidation time is 600 seconds. The right graphs show the differential resistance as a function of a dc bias voltage for a junction at RT and a junction at $T = 150$ mK. The quadratic dependence of the resistance at RT on the dc bias voltage is a good indication of a tunnel barrier [10]. The shift between the two curves (Co-Al = current from Co to Al, Al-Co = current from Al to Co) as a function of bias direction is attributed to the difference in work function between Al and Co [11]. At T= 150 mK a tunnelling behavior is observed, showing the BCS gap and DOS in Al.*

between the two curves in the inset as a function of the bias direction (from Al to Co or vice versa) is a result of the different work functions between Co and Al.

3.4 Fabrication procedure of the individual samples

In this paragraph the fabrication process for two different types of spin valve devices is discussed in detail. The first type are lateral ferromagnetic metal-nonmagnetic metal-ferromagnetic metal (F/N/F) spin valve structures with transparent interfaces. For these devices different ferromagnetic metals, permalloy (Py), cobalt (Co) and nickel (Ni), are used as electrical spin injectors and detectors. For the nonmagnetic metal both aluminium (Al) and copper (Cu) are used.

The second type of devices are lateral $Co/Al_2O_3/Al/Al_2O_3/Co$ spin valves with tunnel barrier contacts.

3.4.1 Design requirements

The aim is to fabricate a lateral spin valve consisting of two ferromagnetic electrodes and a nonmagnetic metal transport channel. Both types of spin valve devices should have the following properties:

- The ferromagnetic electrodes should be single domain over at least the region which is in contact with the normal metal. Multiple domains would mean injection/detection of both spin components, reducing the injection efficiency. In addition the micro-magnets should have a well defined easy axis along which the magnetization aligns. This means that the aspect ratio (length/width) of the micro-magnet should be high (~ 5).

- The micro-magnets should have different coercive ("switching") fields. In this way, parallel and anti-parallel magnetization directions of the micro-magnets can be realized by sweeping the external field from positive to negative values and vice versa. Studies show that the coercive field mainly depends on the width of the electrodes (see Chapter 4) for aspect ratios larger than 4.

- The separation between the electrodes should be variable (200nm - 2μm) in order to measure the length dependence of the spin signal.

In addition the tunnel barrier devices (second type) should have an additional requirement:

- The tunnel barrier resistance should be much higher than the resistance of the normal metal over a spin relaxation length to overcome "conductivity mismatch" [14, 15]. In practice this condition is fulfilled for even the most transparent ($T \approx 1 \cdot 10^{-5}$) tunnel barriers, see Fig. 3.5. On the other hand, the tunnel resistance should not become too high in order to limit the voltage drop over the barrier as an 1-2 nm thick Al_2O_3 barrier breaks down at about 1 Volt [13, 16, 17].

3.4.2 F/N/F spin valve structures

Sample fabrication

P-doped Si $< 100 >$ wafers are used as a substrate material with a 200 nm thermally grown oxide on top. In a first step the basic electrical contact pattern and 10 bond pads consisting of 5 nm Ti and 30 Au are fabricated using UV-optical lithography. In Fig. 3.6 the 10 contact fingers of this optically defined structure can be seen. In between these 10 contact fingers an area of about 30×40 μm^2 is left blank for EBL patterning.

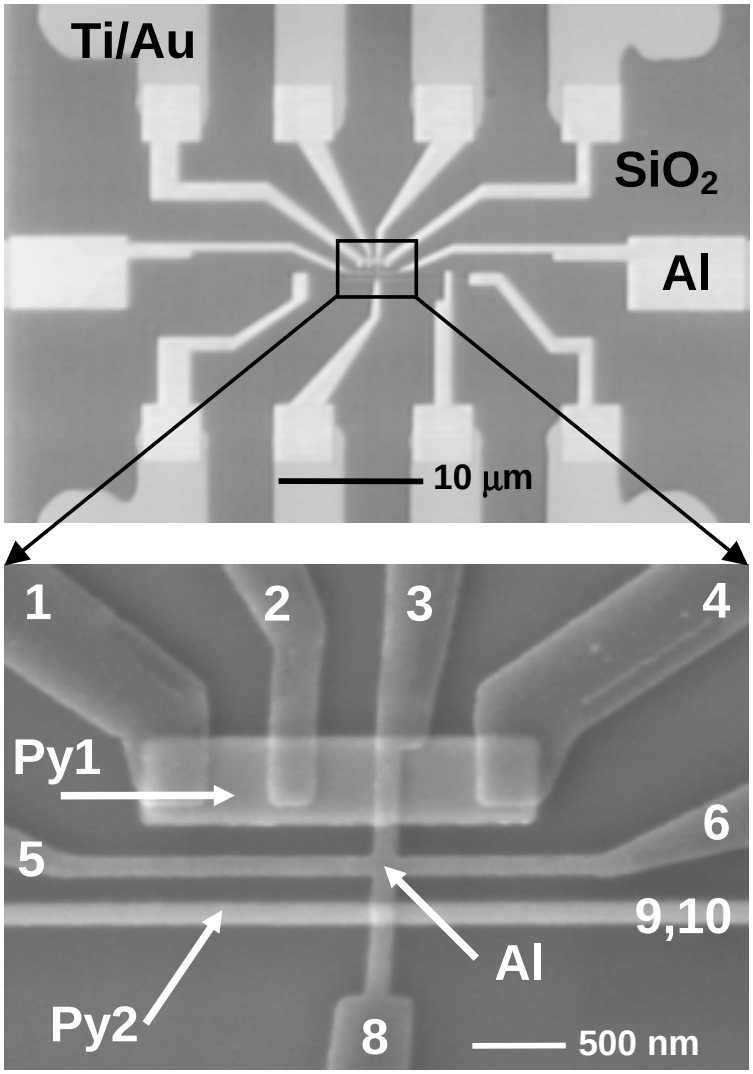

Figure 3.6: *Optical micrograph (top) and a scanning electron microscope (SEM) picture (bottom) of a lateral mesoscopic spin valve device with a ferromagnetic electrode spacing* $L = 500$ *nm. The two horizontal strips are the ferromagnetic electrodes F1 (Py1) and F2 (Py2). Their sizes are* $(2 \times 0.5\ \mu m^2)$ *and* $(14 \times 0.15\ \mu m^2)$ *respectively. An aluminum (Al) cross is placed in between the Py electrodes, which vertical arms lay on top of the Py electrodes. A total of 10 contacts are connected to the device.*

Subsequently the spin valve devices are fabricated in two steps by means of e-beam lithography with a conventional PMMA bi-layer resist and lift-off technique. To avoid magnetic fringe fields, the ferromagnetic electrodes are deposited first. The 40 nm thick Py electrodes are sputter deposited on a 2 nm tantalum (Ta) adhesion layer. The base pressure of the sputter system at IMEC (Belgium) was $2 \cdot 10^{-8}$ mbar vacuum, whereas the background Ar

pressure during sputtering was 1 mbar. A small B-field of 3 mT along the long axis of the Py electrodes was applied during growth in order to align the magneto crystalline anisotropy with the magnetic shape anisotropy of Py electrode. The conductivity of the Py film was determined to be $\sigma_{Py} = 6.6 \cdot 10^6\ \Omega^{-1}m^{-1}$ and $\sigma_{Py} = 1.2 \cdot 10^7\ \Omega^{-1}m^{-1}$ at RT and 4.2 K respectively. The 40 nm thick Co (99.95 % *pure*) and 30 nm thick Ni (99.98 % *pure*) electrodes were deposited by e-gun evaporation in a $1 \cdot 10^{-6}$ mbar vacuum (base pressure: $2 \cdot 10^{-7}$ mbar). The conductivities of the Co and Ni films were determined to be $\sigma_{Co} = 4.2 \cdot 10^6\ \Omega^{-1}m^{-1}$ and $\sigma_{Ni} = 7.6 \cdot 10^6\ \Omega^{-1}m^{-1}$ at RT, whereas at 4.2 K they were $\sigma_{Co} = 7.3 \cdot 10^6\ \Omega^{-1}m^{-1}$ and $\sigma_{Ni} = 1.6 \cdot 10^7\ \Omega^{-1}m^{-1}$. In the second EBL fabrication step, 50 nm thick crossed Cu (99.99 % *pure*) or Al (99.999 % *pure*) strips were deposited by e-gun evaporation in a $1 \cdot 10^{-8}$ mbar vacuum (base pressure: $2 \cdot 10^{-9}$ mbar). Prior to the Cu or Al deposition, a few nm of Py, Co or Ni material was removed from the ferromagnetic electrodes by Kaufmann etching at 500 Volt for 30 seconds in a $2 \cdot 10^{-4}$ mbar Ar environment, thereby removing the oxide to ensure transparent contacts (see Fig. 3.4). The time in between the Kaufmann sputtering and Cu or Al deposition was about 3 minutes. The conductivities of the Cu and Al films were determined to be $\sigma_{Cu} = 3.5 \cdot 10^7\ \Omega^{-1}m^{-1}$ and $\sigma_{Al} = 3.1 \cdot 10^7\ \Omega^{-1}m^{-1}$ at RT, whereas at 4.2 K they were $\sigma_{Cu} = 7.1 \cdot 10^7\ \Omega^{-1}m^{-1}$ and $\sigma_{Al} = 8.0 \cdot 10^7\ \Omega^{-1}m^{-1}$.

Measurement geometry

Two different measurement geometries are used to measure the spin valve effect in the F/N/F device structures, the so called 'conventional' geometry (Fig. 3.7a) and 'non-local' geometry (Fig. 3.7b). In the conventional measurement geometry the current is sent from contact 1 to 7 and the signal $R = V/I$ is measured between contacts 4 and 9, see Fig. 3.6. The conventional geometry suffers from a relatively large background resistance as compared to the spin valve resistance. Small parts of the ferromagnetic electrodes underneath the vertical Cu or Al wires of the cross are included in this background resistance, which can give rise to AMR [18] contributions and Hall effects. These "contact" magnetoresistances of the ferromagnet electrodes can be measured by using the measurement geometries as shown in Fig. 3.7c and 3.7d. Note that in these geometries no spin valve signal can be measured as only one on the ferromagnetic electrodes is involved in the measurement.

In the non-local measurement geometry the current is sent from contact 1 to 5 and the signal $R = V/I$ is measured between contacts 6 and 9. This technique is similar to the "potentiometric" method of Johnson used in Refs. [19–21]. However, the separation of the current and voltage circuits allow us to remove the AMR contribution and Hall effects of the

ferromagnetic electrodes completely: the (magneto) resistance of the current injecting contact (F1) is not relevant because any voltage drop that develops across it will not influence the current that is sent through it and similarly, no current flows through the ferromagnetic voltage contact (F2), so its (magneto) resistance does not effect the voltage measurement. Therefore the only region which could possibly give rise to a magnetoresistance signal is the nonmagnetic metal cross, but explicit measurements confirm that this region does not produce any magnetoresistance. Moreover, this central region would be unable to produce a Hall signal in a non local measurement with a magnetic field perpendicular to the substrate plane as both voltage probes are attached longitudinal to the direction of the current.

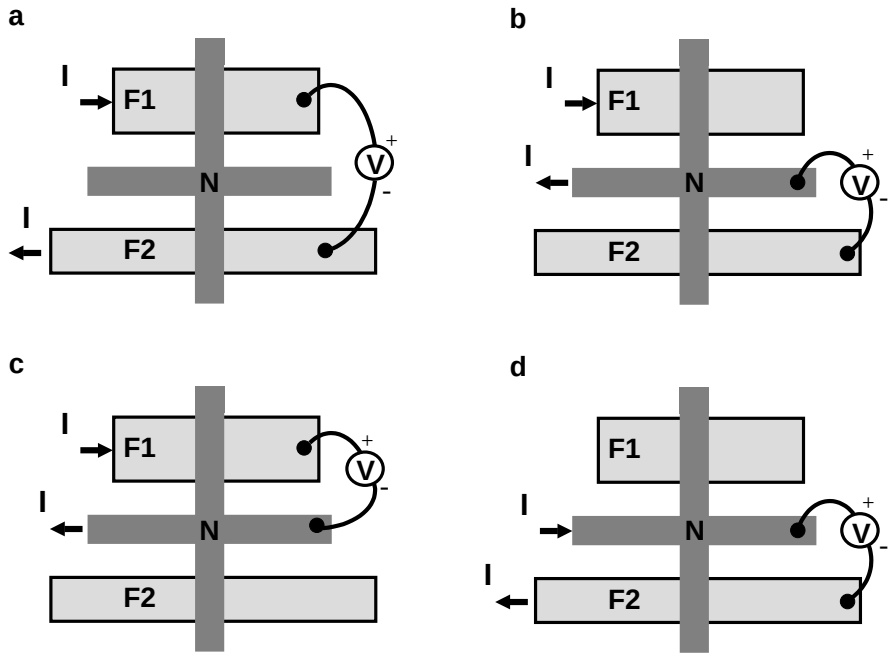

Figure 3.7: *Measurement geometries used for the F/N/F spin valve devices. Spin valve measurements are performed in two geometries, (a) represents the conventional measurement geometry and (b) the non local measurement geometry. The contact magnetoresistance of the ferromagnetic electrode are measured using geometry (c) for the F1 electrode and geometry (d) for the F2 electrode*

3.4.3 F/I/N/I/F spin valve structures

P-doped Si $< 100 >$ wafers are used as a substrate material with a 200 nm thermally grown oxide on top, having the same electrical contact pattern as desbribed in §3.4.2. Subsequently the spin valve devices are fabricated by means of a shadow evaporation process in combination with the PMMA-germanium-MA tri-layer resist mask. Figure 3.8 shows the mask design

which is written in the tri-layer resist by e-beam exposure. The light gray areas are exposed with a low dose, whereas the dark grey and black areas are exposed with a high dose. When the tri-layer resist is developed (see §3.2.2) the light grey areas is Fig. 3.8 form the undercuts of the shadow mask, whereas the dark grey and black regions represent the removed Ge layer. Note that in the middle of Fig. 3.8 the Ge layer forms a fully suspended bridge across the PMMA-MA bottom layer.

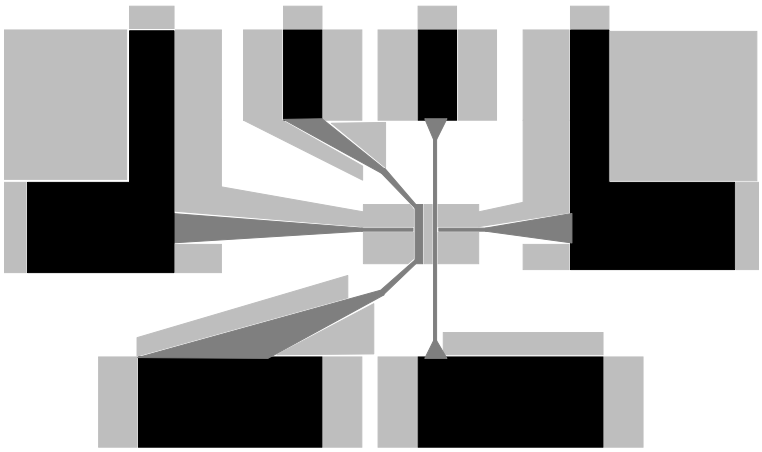

Figure 3.8: *Mask design for the lateral $Co/Al_2O_3/Al/Al_2O_3/Co$ spin valves with tunnel barrier contacts.*

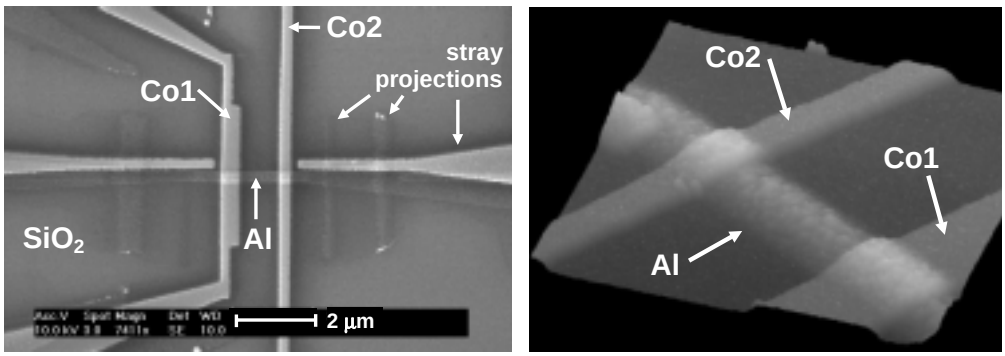

Figure 3.9: *Scanning electron microscope (SEM) picture (right) and an atomic force microscopy (AFM) picture of a lateral $Co/Al_2O_3/Al/Al_2O_3/Co$ spin valve with tunnel barrier contacts with a ferromagnetic Co electrode spacing $L = 1100$ nm.*

After completion of the mask, a two step shadow evaporation procedure is used to make the sample. First we deposit an Al layer from the left and right side of Fig. 3.8 at a pressure of $1 \cdot 10^{-6}$ mbar, under an angle of $\theta = 65°$ with the substrate normal, see also Fig. 3.3. In this way a continuous Al

strip underneath the suspended Ge mask is made with a thickness of 50 nm. Next, without breaking the vacuum, an Al_2O_3 oxide layer is formed at the Al surface due to a 10 minutes O_2 exposure at 5 x 10^{-3} mbar. In a third step, after the vacuum is recovered, two Co electrodes with sizes of $0.4 \times 4\ \mu m^2$ (Co1) and $0.2 \times 12\ \mu m^2$ (Co2) and a thickness of 50 nm are deposited from below Fig. 3.8 under an angle of $\theta = 20°$ with the substrate normal. In Fig. 3.9a a SEM picture is shown of a sample with a Co electrode spacing of $L = 1100$ nm. Dummy or stray shadow projections can also clearly be identified in Fig. 3.9.

The conductivity of the Al strips of the samples used in Ref. [22] was determined to be $\sigma_{Al} = 1.1 \cdot 10^7\ \Omega^{-1}m^{-1}$ at RT and $\sigma_{Al} = 1.7 \cdot 10^7\ \Omega^{-1}m^{-1}$ at $T = 4.2$ K. The conductivity of the Co strips in these samples was determined to be $\sigma_{Co} = 4.1 \cdot 10^6\ \Omega^{-1}m^{-1}$ at RT, whereas the resistance of the $Al/Al_2O_3/Co$ tunnel barriers was typically 600 Ω for the Co1 electrode and 1200 Ω for the Co2 electrode at RT.

3.5 Measurement techniques

The samples are glued to standard 16 pin sample holders using Oxford instruments Varnish. Electrical connection to the samples is made by means of ultrasonic wire bonding using 25 μm Al-Si (1% Si) wires. The sample holders can be placed in a dip-stick for measurements at 1.4 - 4.2 K or in a holder thermally anchored to the mixing chamber of a Kelvinox dilution refrigerator for measurements over 0.1 - 1 K. In both cases copper plates at the lowest temperature surround the sample. For all spin valve measurements at RT and dip-stick measurements at 1.4 - 4.2 K no RC filtering was used. For superconducting tunnelling measurements in a dilution fridge noise filtering is applied, consisting of a single stage home-built RC filter at room temperature and three RC low pass filters in series (each consisting of a 2.7 $k\Omega$ metal film resistance and a 1 nf multilayer capacitance) plus a copper powder filter at the lowest temperature, analogous to the system described in Ref. [23]. The low-pass RC filters have a low frequency cut-off of 60 kHz. At high frequencies, in the order of several 100 MHz, the attenuation of these filters decreases, due to stray capacitances in the resistors. For the filtering of the frequencies above 0.5 GHz the copper powder filter is used.

The connections from the RT or cryogenic system to the measurement setup are done using twisted pairs of co-axial cables. The electrical measurements are performed using voltage controlled current sources and differential voltage amplifiers which are electrically isolated from the environment by means of high frequency magnetic coupling. Standard lock-in detection

techniques to measure AC signals are used in combination with standard multi-meters to measure the output voltage from the amplifiers. The electrical measurements for the spin valves with transparent contacts (F/N/F) are done in a symmetrical mode, which means that the current source applies a voltage from $-\frac{1}{2}V$ to $+\frac{1}{2}$V to send the ac current through the sample and the electrical wiring. Because both electrical leads from the current source to the sample have a much larger resistance ($\approx 100\ \Omega$ each) than the measured (4-terminal) resistance of the sample, the potential at the position of the voltage probes stays close to zero. This makes the detection of the small spin injection signals of the order of $10 - 100$ nV easier to detect, as the common mode signal is easier suppressed by the differential amplifier. However, for the electrical measurements on the $Al/Al_2O_3/Co$ tunnel barrier spin valves it is necessary to use an assymmetrical mode, which means that the current source applies a voltage from 0 to V to send the ac current through the sample and the electrical wiring. The Al strip is connected to the inactive or ground (V=0) terminal of the current source in the asymmetrical mode. Because of the asymmetrical resistance in the current leads, the full potential swing from 0 to V is mostly across the tunnel barrier resistance, leaving the potential of the Al strip close to 0 and hence reducing the common mode signal for the differential amplifier.

The magnetic fields at RT are generated using a GMW 3470 electromagnet which is able to deliver a maximum field of 400 mT with a pole gap distance of 25 mm. At low temperatures ($T < 4.2$ K) higher magnetic fields up to 8 T are achieved with a superconducting magnet.

References

[1] M. Hatzakis, J. Electrochem. Soc. **116**, 1033 (1969).

[2] The mechanism explained is valid for PMMA as well as any positive electron beam resists. Negative resists are also available, where the exposed part becomes insoluble in the developer whereas the unexposed region remain soluble.

[3] T. H. Chang, Vac. Sci. Technol **12**, 1271 (1975).

[4] Depending on the stability of already deposited layers on the sample, a lower baking temperature of both PMMA layers, of the order of 120° can be desirable. However, we did not use this for the devices presented in this work.

[5] L. D. Jackel, R. E. Howard, E. L. Hu, D. M. Tennant, and P. Grabbe, Appl. Phys. Lett. **39**, 268 (1981).

[6] G. J. Dolan, Appl. Phys. Lett. **31**, 337 (1977).

[7] R. Meservey and P. M. Tedrow, Physics Reports **238**, 173 (1994).

[8] I. Giaver, Phys. Rev. Lett **5**, 147 (1960).

[9] J. J. A. Baselmans, Ph.D. thesis, University of Groningen (2002).

[10] J. G. Simmons, J. Appl. Phys. **34**, 1763 (1963).

[11] R. Coehoorn, *Lecture notes 'New magnetoelectronic materials and devices'* (unpublished, 1999), 3 parts.

[12] B. L. Jönsson-Åkerman, R. Escudero, C. Leighton, S. Kim, I. K. Schuller, and D. A. Rabson, Appl. Phys. Lett. **77**, 1870 (2000).

[13] K. Gloos, P. J. Koppinen, and J. P. Pekola, e-print: arXiv:cond-mat/0105511 (2001).

[14] A. Fert and S. Lee, Phys. Rev. B **53**, 6554 (1996).

[15] G. Schmidt, D. Ferrand, L. W. Molenkamp, A. T. Filip, and B. J. van Wees, Phys. Rev. B **62**, R4790 (2000).

[16] W. Oepts, H. J. Verhagen, W. J. M. de Jonge, and R. coehoorn, Appl. Phys. Lett. **73**, 2363 (1998).

[17] R. Coehoorn, private communication.

[18] T. G. S. M. Rijks, R. Coehoorn, M. M. de Jong, and W. J. M. de Jonge, Phys. Rev. B **51**, 283 (1995).

[19] M. Johnson, Science **260**, 320 (1993).

[20] M. Johnson, Phys. Rev. Lett. **70**, 2142 (1993).

[21] M. Johnson, J. Appl. Phys. **75**, 6714 (1994).

[22] F. J. Jedema, H. B. Heersche, A. T. Filip, J. J. A. Baselmans, and B. J. van Wees, Nature **416**, 713 (2002).

[23] J. M. Martinis, M. Devoret, and J. Clarke, Phys. Rev. B **35**, 4682 (1987).